Journal of Zhejiang University-SCIENCE A (Applied Physics & Engineering) in press
www.jzus.zju.edu.cn; www.springer.com/journal/11582
E-mail: jzus_a@zju.edu.cn

Research Article

https://doi.org/10.1631/jzus.A2400437

Manufacturing and thermal properties of steel-carbon fibre/polyetheretherketone (CF/PEEK) hybrid shafts using laser-assisted in-situ consolidation

Zequan DING[1,2], Congcong LUAN[1,2,3]✉, Xinhua YAO[1,2], Lingyu CHENG[4], Yuyang JI[1,2], Chengcheng NIU[1,2], Ningguo DONG[1,2], Kai ZHAO[4], Zhibin RUAN[5], Jianzhong FU[1,2]

[1]*State Key Laboratory of Fluid Power and Mechatronic Systems, College of Mechanical Engineering, Zhejiang University, Hangzhou 310058, China*
[2]*Key Laboratory of 3D Printing Process and Equipment of Zhejiang Province, College of Mechanical Engineering, Zhejiang University, Hangzhou 310058, China*
[3]*State Key Laboratory of Mechanical Transmission for Advanced Equipment, Chongqing University, Chongqing 400044, China*
[4]*Shanghai Aerospace Equipment Manufacturing Co. Ltd, Shanghai 200245, China*
[5]*Zhejiang Advanced CNC Machine Tool Technology Innovation Center Co., Ltd, Taizhou 317500, China*

Abstract: A novel steel-carbon fibre/polyetheretherketone (CF/PEEK) hybrid shaft is proposed, considering the thermal stability, negative coefficient of thermal expansion in fibre orientation and high stiffness of CF/PEEK, which is expected to suppress the thermal deformation of shafts. A laser-assisted in-situ consolidation (LAC) process, together with its equipment, was developed to manufacture the hybrid shaft. Firstly, the optimal process parameters, including the laser-heated temperature and placement speed, were investigated. A maximum short beam shear strength of 80.7 MPa was achieved when the laser-heated temperature was 500 ℃ and the placement speed was 100 mm/s. In addition, the failure modes and the effect of environmental temperature on the CF/PEEK samples were analyzed. Both interlayer cracks and inelastic deformation failure modes were observed. The formation and propagation of cracks were further investigated through digital image correlation (DIC). Furthermore, internal defects of the CF/PEEK sample were detected using X-ray tomography scans, and a minimum porosity of 0.23% was achieved with the optimal process parameters. Finally, two steel-CF/PEEK hybrid shafts, with different fibre orientations, were manufactured based on the optimal process parameters. The surface temperature distributions and thermal deformations were investigated using a self-established deformation/temperature measurement platform. The hybrid shaft showed an 85.7% reduction in radial displacement with hoop fibre orientation and an 11.5% reduction in axial displacement with cross fibre orientation compared with the steel shaft. The results indicate that the proposed method has great potential to improve the thermal stability of hybrid shafts and the accuracy of machine tools.

Key words: Thermal characteristics; Steel-CF/PEEK hybrid shaft; Laser-assisted in-situ consolidation; Thermal deformation; CF/PEEK

1 Introduction

The thermal characteristics of shafts have a significant impact on the accuracy and stability of rotary machines, especially precision machine tools. About 40%-70% of the total manufacturing error is caused by the thermal deformation of the shaft in precision machine tools (Mayr et al., 2012). Passive cooling (Zheng and Chen, 2022; Fan et al., 2022; Lei et al., 2022; Li et al., 2023; Li et al., 2023a), thermal structure optimization design (Xia et al., 2015; Li et al., 2023; Li et al., 2023; Li et al., 2023b), and thermal error compensation (Bao et al., 2023; Li et al., 2023; Lu et al., 2023; Song et al., 2023) are the three main measures used to improve machining accuracy. Thermal structure optimization design is expected to reduce the thermal deformation from the origin, without an external cooling system or sensors. New materials, including ceramics and carbon fibre, have

✉ Congcong LUAN, lccshdg@zju.edu.cn
Zequan DING, https://orcid.org/0009-0005-9287-1325
Congcong LUAN, https://orcid.org/0000-0001-6289-9400

Received Sep. 04, 2024; Revision accepted Dec. 20, 2024; Crosschecked

© Zhejiang University Press 2025

Unedited

been introduced during the optimization of thermal structure design, considering their thermal stability (Vermeulen et al., 2000; Namba, 2001; Ding et al., 2016; Liang et al., 2016; Ge and Ding, 2018).

Polyetheretherketone (PEEK), as a high-performance thermoplastic, is widely applied as the matrix for carbon fibre reinforced composites in mechanical, aerospace, and other fields due to its excellent mechanical properties, high thermostability, corrosion resistance, and shock absorption (Moddeman et al., 1986; Cirino et al., 1987; Grove, 1992; Cebe et al., 2010; Pratte, 2012; Ji et al., 2015). Furthermore, carbon fibre has a negative coefficient of thermal expansion in the fibre direction, which is thought to compensate for thermal deformation. Thus, carbon fibre reinforced polyetheretherketone (CF/PEEK) is considered a great candidate to improve the thermal characteristics of shafts. However, how best to combine CF/PEEK with steel to produce a hybrid shaft needs investigation, and the high melting point (exceeding 340 ℃) and viscosity of PEEK create great challenges to the intimate interface bonding required during the manufacture of steel-CF/PEEK hybrid shafts (Levy et al., 2014; Stokes-Griffin and Compston, 2016; Çelik et al., 2020; Çelik et al., 2021).

Fortunately, rapid heating can be achieved by laser and a high-temperature area of up to 600 ℃ can be acquired within several hundred milliseconds (Stokes-Griffin and Compston, 2015). This can be used as the heating source during the in-situ consolidation process called laser-assisted in-situ consolidation (LAC). The mechanism and behavior of laser irradiation on CF/PEEK prepreg during the LAC process has been investigated in our previous work (Ji et al., 2023). The effects of process parameters, including laser power and placement speed, on the crystallinity and mechanical properties were analyzed in detail. In addition, the effect of the shadow region on the heating temperature distribution was revealed (Jiang et al., 2023). Furthermore, the combined effects of laser power, placement speed, and consolidation force on the shear strength were investigated and a maximum shear strength of 78 MPa was achieved (Comer et al., 2015; Miao et al., 2021). Therefore, the LAC process is expected to realize the intimate interface bonding of steel-CF/PEEK hybrid shafts, although it has never been applied to the manufacture of large curvature structures. Besides, the thermal characteristics, such as thermal deformation and surface temperature distribution of steel-CF/PEEK hybrid shafts manufactured by the LAC process, still need to be investigated and analyzed.

This study aimed to explore the feasibility of steel-CF/PEEK hybrid shafts manufactured by the LAC process. The principle and platform of the hybrid shaft manufacturing process were established. The optimal process parameters were obtained through a series of short beam shear (SBS) strength tests. In addition, failure modes and internal defects were analyzed using digital image correlation (DIC) and X-ray tomography scans. Finally, steel-CF/PEEK hybrid shafts with different fibre orientations were designed and manufactured. Meanwhile, the thermal characteristics of different steel-CF/PEEK hybrid shafts were investigated by comparing them with a steel shaft using a self-developed deformation/temperature measurement platform.

2 Materials and experiments

2.1 Principle and platform of hybrid shaft manufacturing

The principle of hybrid shaft manufacturing using the LAC process is shown in Fig. 1(a). The CF/PEEK prepreg is placed on the steel core shaft under the heating of an NIR laser and pressure provided by the roller. The main principle is that the laser simultaneously irradiates the CF/PEEK prepreg tape and CF/PEEK layer that has already been placed on the steel core shaft, melting the PEEK resin on both surfaces of the CF/PEEK layer and CF/PEEK prepreg tape. Meanwhile, a rubber roller is used to press incoming CF/PEEK prepreg tape on the CF/PEEK layer. Under consolidation force, the melted areas contact each other at the nip point and new molecular chains form between the melted resins, achieving high-strength additive manufacturing of CF/PEEK prepreg tape.

A self-developed LAC process platform based on the above principle was established, including a self-developed LAC placement head, assembled at the end of the sixth axis of the robotic arm (NJ220-2.7, COMAU), and a rotary platform, collaboratively controlled by robotic system, (Fig. 1(b)).

Uncorrected

The steel core shaft is clamped on the rotary platform through a three-jaw chuck, rotating along with the motor. The fibre orientation can be adjusted by controlling the angle between the roller axis and the core shaft axis through the rotation of the robotic arm. The outside surface linear velocity of the core shaft and the roller movement speed along the axis of the core shaft can be obtained based on the optimal placement speed and the angle between the axes of the roller and the core shaft, according to the speed decomposition law.

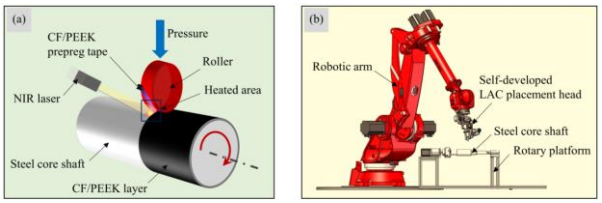

Fig. 1 Hybrid shaft manufacturing with the LAC process: (a)the principle of LAC and (b) the manufacturing platform.

2.2 Materials

In this study, we used T800 CF/PEEK prepreg tape (HENGBO, China) containing 34% mass fraction PEEK. The prepreg tape was 6.35 mm wide and 0.21 mm thick. S45C steel, a medium carbon structural steel, was adopted as the core shaft, considering its compatibility with other machine tool components and overall comprehensive performance. The thermal and mechanical properties of the CF/PEEK and S45C steel are listed in Table 1.

Table 1 Thermal and mechanical properties of T800 CF/PEEK prepreg tape and S45C steel.

	S45C steel	CF/PEEK (longitudinal)	CF/PEEK (Transverse)
Specific heat capacity[J/(kg•K)]	460	1600	1600
Thermal conductivity[W/mK]	50	160	0.64
Emissivity	0.13	0.71	0.71
Coefficient of thermal expansion[1/K]	11.6×10^{-6}	-0.09×10^{-6}	22.4×10^{-6}
Elastic modulus[GPa]	210	243.3	8
Shear modulus[GPa]	80	/	/

3 Results and discussion

3.1 Optimization of LAC process

3.1.1 SBS and DIC test

SBS tests were conducted to investigate the optimal parameters of the LAC process and DIC (MatchID-Stereo HR, China) was applied simultaneously to illustrate the failure mode of samples during SBS tests. The experimental equipment and process are shown in Fig. 2. An electronic universal testing machine UTM5105, fitted with a high/low temperature chamber, was adopted to conduct SBS tests under different ambient temperatures. A customized fixture was used to satisfy the testing condition according to ASTM-2344 (Fig. 2(b)). The loading speed was set at 1 mm/min. Meanwhile, DIC equipment, including two cameras and two LED light sources, was positioned in front of the SBS testing area (Fig. 2(a)). The focal length and depth of field of both cameras were adjusted to ensure that the painting area on the samples was in the same position in the captured images. Before the experiment, a dedicated calibration plate was placed in front of the sample manually and slightly changed positions. Twenty pictures were captured by cameras to calculate the distance between two points in the photos and iterate various algorithms in the software to obtain the best signal-to-noise ratio for sample strain calculation. Subsequently, during SBS tests, the loading process was recorded by cameras, with a sampling frequency of 1 Hz.

A series of CF/PEEK specimens were manufactured at different laser-heated temperatures and placement speeds. The total number of CF/PEEK prepreg tape layers was set to 16, resulting in a series of layers at least 2.4 mm thick. The robotic arm automatically lifted 0.15 mm for manufacturing each ply according to the program to ensure that the laser irradiation position and angle did not deviate. After completing the manufacture of the CF/PEEK prepreg tape, the formed CF/PEEK naturally cooled to room temperature before proceeding with the incoming CF/PEEK prepreg tape. Specific manufacturing process parameters are listed in Table 2, which were determined according to the physical properties of CF/PEEK, reported literature, and our pre-experiments (Ji et al., 2023; Donough et al., 2022; Niu et al., 2024).

Uncited

Table 2 Manufacturing process parameters in SBS tests.

Process parameters	Values
Laser-heated temperature [℃]	400,450,500,550
Placement speed [mm/s]	25, 50, 75, 100
Consolidation pressure [MPa]	0.6
Irradiation angle [°]	24

After manufacturing all CF/PEEK specimens, five samples were prepared for each specimen. The final cross-sectional size of each sample was 2.4◊4.8 mm. The prepared specimens and the dimensions of the samples are shown in Fig. 2(c). Considering the acceleration of the robotic arm movement and the time required for the rollers to reach a stable working temperature, samples were taken at a distance of 200 mm from the starting point to ensure that the performance of samples truly reflected the bonding quality under different process parameters. The SBS of each sample was calculated using the following equation:

$$\sigma_{sbs}=0.75\times F_{max}/(b\times h) \quad (1)$$

where F_{max} is the maximum force recorded in the SBS test, b is the width and h is the thickness of the sample. For the DIC tests, each sample was subjected to spray painting treatment, and small spots were observed on the surface for calculating strain and displacement.

The effect of ambient temperature on the SBS of CF/PEEK was also investigated. Considering the working conditions of the shaft, tests at four ambient temperatures, 40, 50, 60, and 70 ℃, with 60 % humidity, were conducted in a high-low temperature chamber. After samples were put in, it took 20 min for the temperature inside the chamber to reach the set value before starting the SBS test.

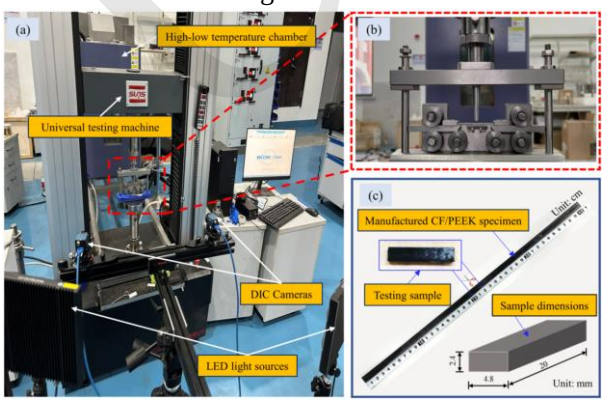

Fig. 2 Short beam strengths and DIC tests: (a) overall testing equipment (b) customized fixture and (c) prepared sample and sample dimensions.

3.1.2 Result of SBS

The influence of laser-heated temperature and placement speed on CF/PEEK SBS is shown in Fig. 3. For the four placement speeds used in the experiment, SBS exhibited two different trends of change. When the process temperature was 400 ℃ or 450 ℃, the SBS gradually decreased with increasing placement speed. On the other hand, when the process temperature exceeded 500 ℃, as the placement speed increased, the SBS first decreased and then increased. The highest SBS of 80.7 MPa was obtained with a 500 ℃ process temperature and 100 mm/s placement speed.

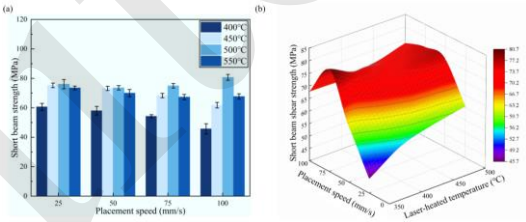

Fig. 3 SBS results: (a) SBS with different laser-heated temperatures and placement speeds, and (b) synthetic influence surface showing the effect of laser-heated temperature and placement speed on interlaminar shear strength.

3.1.3 Failure modes

To further evaluate the manufacturing quality of samples, the failure modes in SBS tests were investigated and analyzed. Both interlayer cracks and inelastic deformation failure modes were observed (Fig. 4). The failure modes were closely related to the load-bearing capabilities, and interlayer cracks appeared on the surface of samples when the SBS was less than 65 MPa (Fig. 4(a)). Samples suffered inelastic deformation instead of cracking when the SBS was greater than 65 MPa (Fig. 4(b)).

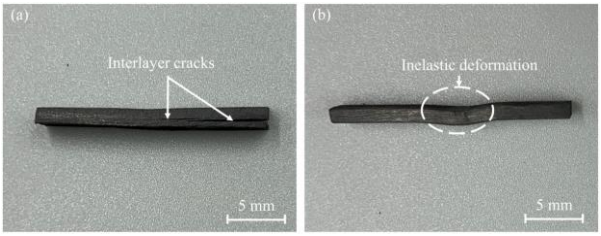

Fig. 4 Two failure modes in SBS tests: (a) interlayer cracks

and (b) inelastic deformation.

Furthermore, the formation and propagation of cracks were investigated by DIC. The maximum principal strain of the sample during the SBS test was observed (Fig. 5). When the load reached a critical value, a large principal strain first appeared in an interface near the loading head directly below the force point, indicating the generation of a crack (Fig. 5(a)). Under the action of the loading head, the sample underwent bending, and different layers of CF/PEEK were subjected to different principal stresses. Since the interface bonding quality was relatively weak, it was prone to produce large strains at interfaces due to the lack of carbon fibres providing greater stiffness. Thus, the undamaged interlayer area exhibited greater strain than adjacent areas. As the load increased further, the principal strain located at the same interface gradually increased and extended towards the end face of the sample (Fig. 5(b)). After 300 s loading, a new large principal strain area was observed on the left side below the loading area (Fig. 5(c)). Subsequently, for all cracking interlayers, the areas of the large principal strain were extended further along the interface. A new large principal strain interface appeared at the bottom of the sample and to the right of the loading area indicating that a new crack had formed (Fig. 5(d)). 416 s after loading began, the newly formed crack rapidly propagated to the right end of the sample, forming a complete notch (Fig. 5(e)). The entire testing period finished after 688 s of loading. The final sample morphology, with multiple interlayer cracking failures, is shown in Fig. 5(f). All cracks underwent a similar formation propagation process until the end of loading. The upper and lower surfaces of some cracks were refitted under increasing loads, especially in the area adjacent to the centre loading areas. All failure positions were equidistant and parallel to the fibre direction at the interlayer areas, indicating that interlayer strength has a significant impact on the load-bearing capacity of CF/PEEK structures.

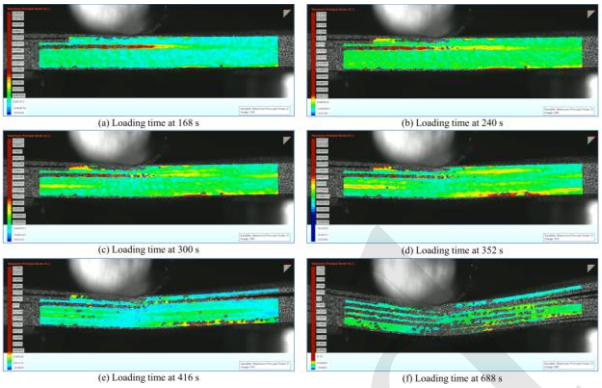

Fig. 5 Crack formation and propagation of samples revealed by DIC.

Based on the location of one crack, the crack opening data of each point on the crack were extracted (Fig. 6). Before the crack appeared, each point on the selected crack barely moved in the observed plane (red line). In the crack expansion stage, as the load increased, the distance between the upper and lower surfaces significantly increased at a certain moment, indicating the sudden formation of the crack (green line). The opening distance tended to decrease from one end to the centre of the sample. The propagation of cracks had a unified characteristic once the initial crack appeared. We attributed this to the high stiffness of the CF/PEEK along the fibre direction, maintaining a relatively stable failure morphology on both sides of the fracture. The displacement of each point increased uniformly along the crack until the maximum displacement of 0.1046 mm was reached (blue line). At this stage, stress was released through the continuous expansion of cracks to withstand gradually increasing pressure. After that, with a further increase in pressure force, the crack opening distance began to decrease. The upper and lower sides of the crack tended to contact again, and the sample continued to withstand external loads as an entire part. To further investigate the fracture behavior of CF/PEEK composites manufactured using the LAC process, the failure morphology of cracks was analyzed using a field emission scanning electronic microscope (FESEM, Zeiss G300, Fig. 7). Debonding of the interface between the carbon fibres and PEEK matrix was observed accompanying the cracking of the PEEK matrix, indicating that a good interlayer bonding quality was achieved. However, the interface between the carbon fibres and the PEEK matrix needs further improvement.

Uncorrected

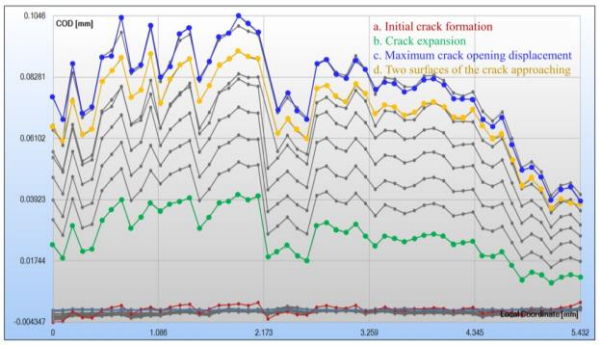

Fig. 6 Crack propagation of samples during SBS tests.

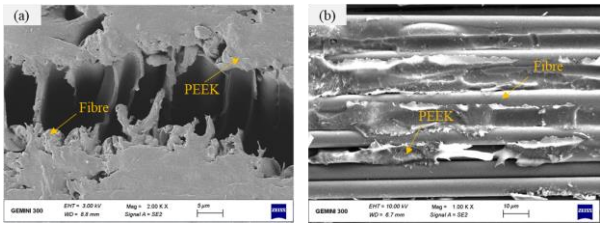

Fig. 7 The failure morphology of cracks: (a) cross section and (b) surface of a crack.

3.1.4 Internal defects

To further characterize the performance of interface bonding, the internal defects of two samples, manufactured at 400 ℃, 75 mm/s and 500 ℃, 100 mm/s, respectively, were detected through three-dimensional X-ray tomography scans (Xradia 515 Versa, Zeiss). The voxel size was set at 1 μm^3 during 3D X-ray scanning. Carbon fibres, PEEK and voids could be clearly distinguished due to their different optical properties and the obtained data were used for 3D reconstruction to generate a 3D structure of the local area. 1000 slices were obtained for 3D reconstruction of the whole scanning region. The porosity of the detected area of the CF/PEEK sample was calculated using Dragonfly Pro analysis software.

For the sample manufactured with 400 ℃ and 75 mm/s process parameters, five interlayers, formed by the enrichment of PEEK, and the interior of the carbon fibre prepreg can be observed (Fig. 8). A porosity of 0.23% was achieved for the CF/PEEK component and a void enrichment area was observed at interface-*iii*, with a maximum void width of 8.9 μm. Further observation of interface-*iii* revealed a series of defects arranged along the carbon fibres near this void, as well as a fibre with an inconsistent arrangement direction. This may have been due to fluctuation in the surface quality and PEEK content. However, voids deteriorate the performance of CF/PEEK structural components and can become the source of cracking failure.

A cross-section view of the sample, manufactured with the optimal process parameters, is shown in Fig. 8(b). There is no obvious interlayer area. All carbon fibres are evenly distributed throughout the entire observation field, indicating that the load-bearing capacity of the entire section is uniform and the load-bearing capacity of the sample is enhanced. Therefore, the inelastic deformation failure mode is inclined to appear. The porosity was also calculated. Only 0.01% volume of voids was detected, proving that the quality of the entire CF/PEEK sample, manufactured with optimal parameters, is reliable.

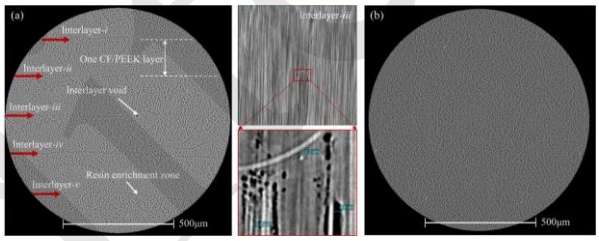

Fig. 8 X-ray tomography of CF/PEEK sample: (a) manufactured with 400 ℃ and 75 mm/s process parameters and the amplification of interlayer-*iii* and (b) manufactured with 500 ℃ and 100 mm/s process parameters.

3.1.5 Effect of ambient temperature on SBS

To investigate the effect of ambient temperature on the performance of CF/PEEK, the SBS of samples manufactured with the optimal parameters under different ambient temperatures was tested (Fig. 9). The SBS decreased slightly with increasing ambient temperature. There was about a 4.3% decline when the temperature rose to 70 ℃, compared with the highest SBS of the sample at 20 ℃. In addition, inelastic deformation failure was observed for all tested samples, indicating that the ambient temperature did not significantly affect the interlayer bonding quality. It also showed that CF/PEEK can be used in steel-CF/PEEK hybrid shafts, which usually operate below 70 °C, because of its good thermal stability.

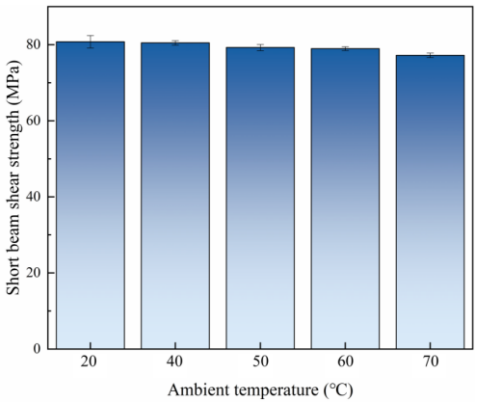

Fig. 9 The effect of ambient temperature on CF/PEEK short beam strength

3.2 Manufacturing of steel-CF/PEEK hybrid shaft

To verify the effect of CF/PEEK on shaft thermal deformation, a 3-mm thick CF/PEEK part was introduced to replace a portion of S45C steel on the outside part of the steel core shaft in the middle area between the bearing areas I and II, with two fibre orientation arrangement methods, respectively (Fig. 10(a)). The two methods included a hoop-orientation arrangement and a cross-orientation arrangement. In the hoop-orientation arrangement, the carbon fibres maintain a consistent circumferential, namely at 90 ° to the centerline of the core shaft. In the cross-orientation arrangement, the CF/PEEK prepreg tapes are stacked in a ±45 °sequence. The first layer CF/PEEK for two hybrid shafts was arranged in cross-orientation orientation. For the first steel-CF/PEEK hybrid shaft, all CF/PEEK prepreg tapes were arranged in the hoop-orientation and for the second they were arranged in the cross-orientation, except for the first layer. The specifications of the steel-CF/PEEK hybrid shaft are shown in Fig.10(b). For comparison, a steel shaft of the same size was made using S45C steel as a reference.

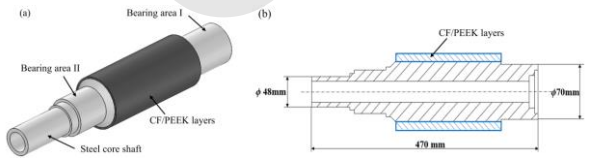

Fig. 10 Schematic of a steel-CF/PEEK hybrid shaft (a) CF/PEEK position on the shaft and (b) specific dimensions schematic diagram.

Steel-CF/PEEK hybrid shafts were manufactured using the self-developed manufacturing platform (Fig. 11(a)). The steel core shaft (Fig. 11(b)), was manufactured in advance using a traditional mechanical processing method. For further CF/PEEK manufacturing, the LAC process was applied, with the optimal combination of laser-heat temperature and placement speed. A robotic arm drove the LAC placement head to press CF/PEEK prepreg tape at the starting point of the path, and then the robotic arm and core shaft, both axes of which were adjusted to a certain angle, rotated at the set speed, in conjunction with the function of the laser, to complete the entire CF/PEEK manufacturing process. The manufacture of cross-orientation and hoop-orientation CF/PEEK is shown in Fig. 11(c) and Fig. 11(d), respectively. Finally, steel-CF/PEEK hybrid shafts, with cross-orientation and hoop-orientation, are shown in Fig. 11(e) and Fig. 11(f), respectively.

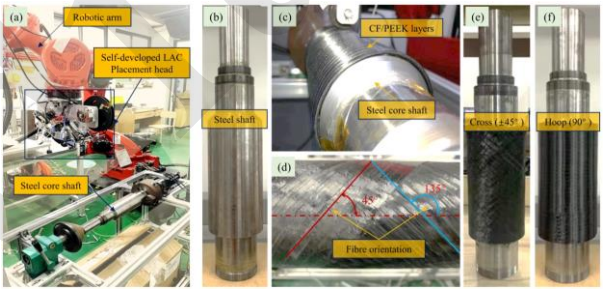

Fig. 11 The manufacture of steel-CF/PEEK hybrid shafts: (a) the additive manufacturing platform before the manufacturing process, (b) steel core shaft, (c) manufacturing according to hoop-orientation, (d) manufacturing according to cross-orientation, (e) hybrid shaft with cross-orientation and (f) hybrid shaft with hoop-orientation.

3.3 Thermal properties of steel-CF/PEEK hybrid shafts

To evaluate the thermal characteristics of the two steel-CF/PEEK hybrid shafts and the steel shaft, a thermal deformation/temperature measurement platform was established to detect the axial thermal deformation and surface temperature of the shafts (Fig. 12). During the measurement process, shafts were placed on a flat insulation plate to minimize heat loss through thermal conduction. Shafts were heated using two silicone rubber heaters fixed on the outside surfaces of bearing areas I and II, simulating the frictional heat under actual working conditions. The heating temperature could be controlled within ±1 ℃

Uncorrected

of the setting value. In this experiment, the heating areas were heated from 20 to 70 ℃. Meanwhile, laser Doppler interferometers were used to measure the axial and radial thermal deformations once the two silicone rubber heaters operated. The laser emitted a single-frequency beam into a linear interferometer, which was then divided into two beams. One spectroscope was attached to the end of the shaft and another to the outer surface of the shaft between two bearing areas. The corresponding laser provided a vertical laser. The signal acquisition system calculated the amount of deformation according to the difference between the original beam and the spectroscope-reflected beam. Five temperature sensors, labelled T1 to T5, were arranged on the outside surfaces of the detecting shaft to measure the surface temperature, and two temperature sensors, labelled T6 and T7, were arranged on a steel frame support to measure the environmental temperature changes of the workbench to eliminate errors. The measurement time was set to 8000 s and the sampling frequency was 1 Hz.

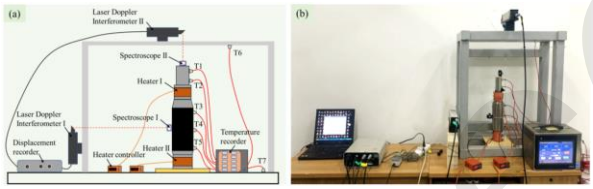

Fig. 12 Deformation/temperature measurement platform: (a) schematic image and (b) physical image.

The surface temperature distributions of two hybrid shafts and a steel shaft are shown in Fig. 13(a,b,c) and a comparison of detection-point temperatures is shown in Fig. 13(d). For detection points T1 and T2, an identical temperature distribution was observed for all three shafts, around 52 ℃ for T1 and 56.8 ℃ for T2. Due to the absence of carbon fibres in this area, the temperature depends mainly on the specific heat capacity of the steel and the convective heat dissipation of the air. However, the temperature measured by T2 on the two hybrid shafts was the highest, while on the steel shaft it was a relatively low-temperature point. The heat dissipation in the area between the two bearing areas was limited due to the insulation plate reducing convection in the centre channel of all three shafts, resulting in a large temperature rise at points T3, T4 and T5 on the steel shaft. Overall, the decrease in surface temperature at the CF/PEEK covered area ranged from 14.7 to 18.2%. Precisely, at T3, T4 and T5 the temperature decreased from 58.4, 56.9, and 56.8 ℃ for the steel shaft to 47.8, 48.5, 47.6 ℃ for the steel-CF/PEEK hybrid shaft with cross-orientation and 48.2, 48.4, and 46.3 ℃ for the steel-CF/PEEK hybrid shaft with hoop-orientation. In addition to the effect of convection heat transfer, CF/PEEK prepreg tapes not only have a larger specific heat capacity but also have an emissivity of 0.71 while the emissivity of S45C steel at room temperature is about 0.13, resulting in a decrease in surface temperature.

Although the temperature difference between the corresponding temperature measurement points was not significant, temperatures at three measurement points on the steel-CF/PEEK hybrid shaft with a cross-orientation arrangement were lower than those of the steel-CF/PEEK hybrid shaft with a hoop-orientation arrangement. The thermal conductivity of carbon fibres along the fibre direction is about three times that of steel. When the cross-orientation arrangement was applied, the entire CF/PEEK area had higher thermal conductivity along the axis direction, resulting in a more uniform temperature distribution on the outside surface of the CF/PEEK layer. Therefore, the high thermal conductivity of carbon fibre could be used to transfer the heat at the contact interface between the shaft and bearings to the outside surface of the CF/PEEK covered area in contact with air for rapid heat dissipation. The uniform distribution of surface temperature also indicates that the temperature distribution inside the carbon fibre layer is relatively uniform along the axial direction. This will help improve the design and theory of hybrid shafts in future work.

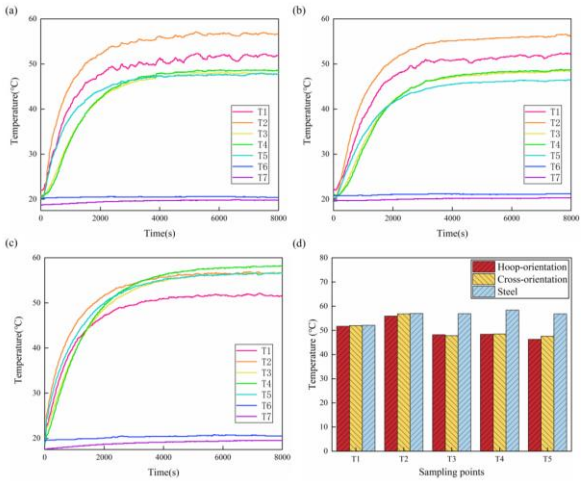

Fig. 13 The surface temperature of (a) a hybrid shaft with cross-orientation CF/PEEK, (b) a hybrid shaft with hoop-orientation CF/PEEK, and (c) a steel shaft, and (d) a comparison of five points temperatures.

The axial and radial thermal deformation of the two hybrid shafts and the steel shaft were measured (Fig. 14). Compared with the steel shaft, the thermal displacement in the axial direction of the hybrid shaft with cross-orientation arrangement was decreased by about 11.5%, from 279 μm to 247 μm, while the axial displacement of the hybrid shaft with hoop-orientation arrangement was increased by about a 16.8%, to 326 μm (Fig. 14(a)). This indicates that a larger proportion of carbon fibres arranged along the axis direction leads to a more significant impact on restricting axial thermal deformation of the steel-CF/PEEK hybrid shaft. On the other hand, high-module carbon fibre, as well as the characteristics of thermal shrinkage in the fibre direction, restricted the deformation in the radial direction. Therefore, the thermal expansion of the hybrid shaft with the hoop-orientation arrangement in the axial direction was more pronounced.

For radial displacement measurement, the experimental conditions were identical to those used for the measurement of axial deformation. According to the results, the radial deformation of the S45C steel shaft was 54.1 μm while the radial deformation of the steel-CF/PEEK hybrid shaft was 7.7 μm with hoop-orientation and 17.7 μm with cross-orientation arrangement, namely a 85.7% and 67.3% reduction, respectively (Fig. 14(b)). This indicates that the hoop-orientation method has a remarkable effect on suppressing radial deformation. As for the steel-CF/PEEK hybrid shaft with cross-orientation, although only one layer of CF/PEEK prepreg tape was arranged at a 90 °angle to the axis, it still had a restraining effect on radial deformation.

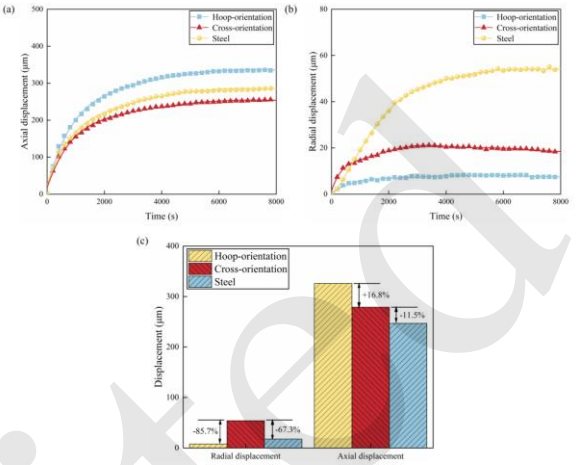

Fig. 14 The displacement of the three shafts:(a) axial displacement, (b) radial displacement and (c) a comparison of displacement.

4 Conclusions

A novel steel-carbon fibre/polyetheretherketone (CF/PEEK) hybrid shaft was proposed and manufactured using a laser-assisted in-situ consolidation process. Firstly, the optimal process parameters were investigated through SBS tests. The highest SBS of 80.7 MPa was acquired at a process temperature of 500 ℃ and a placement speed of 100 mm/s. In addition, two failure modes of interlayer cracks and inelastic deformation for SBS samples were observed, and the inelastic deformation was associated with a higher SBS. Furthermore, crack propagation was analyzed using DIC, and a maximum crack of 0.1046 mm was observed. Meanwhile, the internal defects and porosities of two samples with different process parameters were measured through X-ray tomography. A porosity of 0.23% with clear interlayer resin enrichment areas was found within the sample manufactured at 400 ℃ with a 75 mm/s placement speed, while a porosity of only 0.01% without a resin enrichment area was acquired when the sample was manufactured with optimal parameters of 500 ℃ and 100 mm/s. Finally, two hybrid shafts, with different fibre arrangements, were manufactured with the optimal process parameters. Their surface temperature distributions and thermal displacements were meas-

Uncorrected

ured and compared with those of the steel shaft. The surface temperature decreased by from 14.7% to 18.2% at the CF/PEEK covered area compared with the steel shaft. An 11.5% decrease of axial deformation for the steel-CF/PEEK hybrid shaft with cross-orientation was achieved, compared to the steel shaft. Moreover, for the steel-CF/PEEK hybrid shaft the radial displacement decreased by 67.3% with cross-orientation and by 85.7% with hoop-orientation. Therefore, the proposed steel-CF/PEEK hybrid shaft together with the manufacturing process shows great potential for suppressing shaft thermal deformation.

Acknowledgements

This work was supported by the National Nature Science Foundation of China (No. 52175440), the Aeronautics Science Foundation of China (2023Z049076001), the Science and Technology Innovation Fund of Shanghai Aerospace (SAST2022-060), the Open Fund of State Key Laboratory of Mechanical Transmissions (SKLMT-MSKFKT-202202), the Key R&D Program of Zhejiang Province (2023C01058), and the Experimental Technique Project of Zhejiang University (SYBJS202302).

Author contributions

Zequan DING: Methodology, Visualization, Investigation, Writing-Original draft. Congcong LUAN, Xinhua YAO, and Jianzhong FU: Conceptualization, Supervision, Project administration, Funding acquisition, Resources, Writing-Review & Editing. Yuyang JI, Chengcheng NIU, and Ningguo DONG: Data curation, Visualization, Investigation. Lingyu CHENG, Kai ZHAO, and Zhibin RUAN: Visualization.

Conflict of interest

Zequan DING, Congcong LUAN, Xinhua YAO, Lingyu CHENG, Yuyang JI, Chengcheng NIU, Ningguo DONG, Kai ZHAO, Zhibin RUAN and Jianzhong FU declare that they have no conflict of interest.

References

Mayr J, Jedrzejewski J, Uhlmann E, et al., 2012. Thermal issues in machine tools. *CIRP ANNALS-Manufacturing Technology*,61(2):771-791. https://doi.org/10.1016/j.cirp.2012.05.008

Li M, Ma C, Zeng S, et al., 2023. Cooling water jacket design of motorized spindle system using multi-objective topology optimization. *Applied Thermal Engineering*, 224:120-122. https://doi.org/10.1016/j.applthermaleng.2023.120112

Zheng DX, Chen WF, 2022. Effect of a cooling unit on high-speed motorized spindle temperature with a scaling factor. *International Journal of Advanced Manufacturing Technology*, 120(3-4): 2559-2572. https://doi.org/10.1007/s00170-022-08958-y

Lei M, Gao F, Li Y, Xia P, Wang M. Wan, Yang J, 2022. Feedback control–based active cooling with pre-estimated reliability for stabilizing the thermal error of a precision mechanical spindle. *International Journal of Advanced Manufacturing Technology*,121(3-4): 2023-2040. https://doi.org/10.1007/s00170-022-09471-y

Li Z, Wang B, Zhu W, et al., 2023a. Design and thermal characteristic analysis of motorized spindle cooling water jacket. *International Journal of Advanced Manufacturing Technology*, 128(7-8): 3331-3342. https://doi.org/ 10.1007/s00170-023-12162-x

Fan, K., R. Xu, R. Wang, et al., 2022. Thermoelectric-based cooling system for high-speed motorized spindle II: Optimization and validation strategy. International Journal of Advanced Manufacturing Technology, 119(9-10): 6521-6533. https://doi.org/10.1007/s00170-022-08709-z

Xia, C., Fu JZ, Lai JT, Yao XH, Chen ZC, 2015. Conjugate heat transfer in fractal tree-like channels network heat sink for high-speed motorized spindle cooling. *Applied Thermal Engineering*,90:1032-1042. https://doi.org/10.1016/j.applthermaleng.2015.07.024

Li Z, Wang B, Zhu W, et al., 2023b. Design and thermal characteristic analysis of motorized spindle cooling water jacket. *International Journal of Advanced Manufacturing Technology*, 128(7-8): 3331-3342. https://doi.org/10.1007/s00170-023-12162-x

Li M, Ma C, Liu J, 2023. Topology optimization design of cooling water jacket structure for highspeed spindle-bearing system. *Journal of Manufacturing Process*, 102: 1-22. https://doi.org/10.1016/j.jmapro.2023.07.034

Li Y, Liu Z, Li L, et al., 2023. Topology Structural Design and Thermal Characteristics Analysis of High-Efficiency Heat Conductive Path for the Spindle System. *Processes*, 11(9):2650. https://doi.org/ 10.3390/pr11092650

Li Y, Bai Y, Hou Z, et al., 2023. Thermal error modeling and compensation of spindle based on gate recurrent unit network. *International Journal of Advanced Manufacturing Technology*, 128: 5519–5528. https://doi.org/10.1007/s00170-023-12276-2

Song L, Liu K, Zhao D, et al., 2023. The spindle axial time-varying thermal error compensation method for horizontal boring and milling machine tool based on edge computing. *International Journal of Advanced Manufacturing Technology*, 128(5-6):2631-2638. https://doi.org/10.1007/s00170-023-11927-8

Bao L, Xu Y, Zhou Q, et al., 2023. Thermal Error Modeling of Numerical Control Machine Based on Beetle Antennae Search Back-propagation Neural Networks. *International Journal of Computational Intelligence Systems*,16(1):84. https://doi.org/10.1007/s44196-023-00263-0].

Lu Q, Zhu D, Wang M, Li M, 2023. Digital Twin-Driven

Uncorrected

Thermal Error Prediction for CNC Machine Tool Spindle. *Lubricants*, 11(5):219. https://doi.org/10.3390/lubricants11050219

Vermeulen J, Rosielle P, Schellekens P, 2000. An advanced ceramic optical diamond turning machine design and prototype development. *CIRP ANNALS Manufacturing Technology*, 407-410. https://doi.org/10.1016/S0007-8506(07)62976-X

Ge Z, Ding X, 2018. Design of thermal error control system for high-speed motorized spindle based on thermal contraction of CFRP. *International Journal of Machine Tools & Manufacture: Design, research and application*, 125:99-111. https://doi.org/10.1016/j.ijmachtools.2017.11.002

Namba Y, 2001. 124 Breakage of Glass-Ceramic Spindle of Zero-Thermal-Expansion. The Proceedings of The Manufacturing & Machine Tool Conference 2001.3: 167-168. https://doi.org/10.1299/jsmemmt.2001.3.167

Liang XU, Xie YJ, Ding JT, et al., 2016. The Design and Optimization of carbon fiber laminates based on thermal stability and bending rigidity. *Composites Science and engineering*, (2): 57-61. https://api.semanticscholar.org/CorpusID:139216436

Ding J, Xu L, Ma Z, et al., 2016. The lightweight structure design of a CFRP mirror. AOMATT. https://doi.org/10.1117/12.2243440

Grove S, 1992. Thermoplastic aromatic polymer composites: a study of the structure, processing, and properties of carbon fibre reinforced polyetheretherketone and related materials. *Composites Manufacturing*, 4(1): 59. https://doi.org/10.1016/0956-7143(93)90018-4

Pratte J, 2012. Polyetheretherketone (PEEK) Composites: An Update on Processing-Morphology-Property Relationships., Wiley Encyclopedia of Composites, p.1-16. https://doi.org/10.1002/9781118097298.weoc175

Ji S, Yu H, Zhao J, et al., 2015. Comparison of mechanical property and machinability for polyetheretherketone and glass fiber-reinforced polyetheretherketone. *Advances in Mechanical Engineering*, 7(4). https://doi.org/10.1177/1687814015578357]

Cirino M, Pipes RB, Friedrich K, 1987. The abrasive wear behaviour of continuous fibre polymer composites. *Journal of Materials Science*, 22(7): 2481-2492. https://doi.org/10.1007/BF01082134

Cebe P, Chung SY, Hong SD, 2010. Effect of thermal history on mechanical properties of polyetheretherketone below the glass transition temperature. *Journal of Applied Polymer Science*, 33(2):487-503 https://doi.org/10.1002/app.1987.070330217].

Moddeman WE, Bowling WC, Tibbitts EE, et al., 1986. Thermal stability and compatibility of polyetheretherketone (PEEK) with an oxidizer and pyrotechnic blend. *Polymer Engineering & Science*, 26(21):1469-1477 https://doi.org/10.1002/pen.760262102

Stokes-Griffin CM, Compston P, 2016. Investigation of sub-melt temperature bonding of carbon-fibre/PEEK in an automated laser tape placement process. *Composites Part A: Applied Science and Manufacturing*, 84: 17-25. https://doi.org/10.1016/j.compositesa.2015.12.019

Levy A, Heider D, Tierney J, Gillespie JW, 2014. Inter-layer thermal contact resistance evolution with the degree of intimate contact in the processing of thermoplastic composite laminates. *Journal of Composite Materials*, 48(4): 491-503. https://doi.org/10.1177/0021998313476318

Çelik O, Peeters D, Dransfeld C, et al., 2020. Intimate contact development during laser assisted fiber placement: Microstructure and effect of process parameters. *Composites Part A: Applied Science and Manufacturing*,134: 105888. https://doi.org/10.1016/j.compositesa.2020.105888

Çelik O, Hosseini SMA, Baran I, et al., 2021. The influence of inter-laminar thermal contact resistance on the cooling of material during laser assisted fiber placement. *Composites Part A: Applied Science and Manufacturing*, 145: 106367. https://doi.org/10.1016/j.compositesa.2021.106367].

Stokes-Griffin CM, Compston P, 2015. The effect of processing temperature and placement rate on the short beam strength of carbon fibre–PEEK manufactured using a laser tape placement process. *Composites Part A: Applied Science and Manufacturing*, 78: 274-283. https://doi.org/10.1016/j.compositesa.2015.08.008

Ji YY, Luan CC, Yao XH, et al., 2023. Mechanism and behavior of laser irradiation on carbon fiber reinforced polyetheretherketone (CF / PEEK) during the laser-assisted in-situ consolidation additive manufacturing process. *Additive Manufacturing*, 74:103713. https://doi.org/10.1016/j.addma.2023.103713

Jiang W, Chen C, Chen Z, et al., 2023. Effect of crystallinity on optical properties of PEEK prepreg tapes for laser-assisted automated fiber placement. *Composites Communications*, 38: 101490. https://doi.org/10.1016/j.coco.2022.101490

Miao Q, Dai Z, Ma G, et al., 2021. Effect of consolidation force on interlaminar shear strength of CF /PEEK laminates manufactured by laser-assisted forming. *Composite Structures*, 266:113779. https://doi.org/10.1016/j.compstruct.2021.113779

Comer AJ, Ray D, Obande WO, et al., 2015. Mechanical characterisation of carbon fibre–PEEK manufactured by laser-assisted automated-tape-placement and autoclave. *Composites Part A: Applied Science and Manufacturing*, 69: 10-20. https://doi.org/10.1016/j.compositesa.2014.10.003

Donough MJ, Shafaq, John NA, et al., 2022. Process modelling of In-situ consolidated thermoplastic composite by automated fibre placement – A review. *Composites Part A: Applied Science and Manufacturing*. 163:107179. https://doi.org/10.1016/j.compositesa.2022.107179

Niu CC, Shen HY, Luan CC, et al., 2024. Optimization and assessment of CF/PEEK-PEEK composite shell manufactured by the laser-assisted in situ consolidation inte-

grated with material extrusion process. *Journal of Manufacturing Process*. 119: 452-462.
https://doi.org/10.1016/j.jmapro.2024.03.100

中文概要

题　目：激光辅助原位固结钢-碳纤维/聚醚醚酮（CF/PEEK）复合轴的制造和热特性

作　者：丁泽泉[1,2]，栾丛丛[1,2,3]，姚鑫骅[1,2]，程灵钰[4]，纪毓杨[1,2]，牛成成[1,2]，董宁国[1,2]，赵凯[4]，阮志斌[5]，傅建中[1,2]

机　构：[1]浙江大学，流体动力基础件与机电系统全国重点实验室，中国杭州，310058；[2]浙江大学，浙江省三维打印工艺与装备重点实验室，中国杭州，310058；[3]重庆大学，高端装备机械传动全国重点实验室，中国重庆，400044；[4]上海航天设备制造总厂有限公司，中国上海，200245；[5]浙江先端数控机床技术创新中心有限公司，中国台州，317500

目　的：文章的研究目的是探索一种新型的钢-碳纤维/聚醚醚酮（CF/PEEK）复合轴的制造方法和热特性。该复合轴旨在利用 CF/PEEK 的热稳定性、负轴向热膨胀系数和高刚性来抑制轴的热变形，从而提高旋转机械（尤其是精密机床）的精度和稳定性。

创新点：1. 开发了一种激光辅助原位固化（LAC）工艺及其设备，用于制造复合轴，解决了 PEEK 高熔点和粘度带来的界面结合难题.；2. 建立了自研的变形/温度测量平台，详细研究了不同纤维取向的钢-CF/PEEK 复合轴的表面温度分布和热变形特性，为复合轴的设计和应用提供了理论支持。

方　法：1. 通过 SBS 测试确定 LAC 工艺的最优参数，包括激光加热温度和铺放速度；2. 利用 DIC 技术观察 SBS 测试过程中样品的失效模式，分析裂纹的形成和扩展过程；3. 采用 X 射线断层扫描技术检测 CF/PEEK 样品的内部缺陷和孔隙率；4. 使用自研的变形/温度测量平台，测量不同纤维取向的钢-CF/PEEK 复合轴的表面温度分布和热变形，与钢轴进行对比分析。

结　论：1. 在激光加热温度为 500℃、放置速度为 100 mm/s 时，CF/PEEK 的 SBS 强度达到最大值 80.7 MPa，表明该工艺参数组合为最优；2. 观察到两种失效模式：层间裂纹和非弹性变形，且非弹性变形与较高的 SBS 相关；3. 在最优工艺参数下制造的 CF/PEEK 样品孔隙率仅为 0.01%，无明显的树脂富集区，质量可靠；4. 与钢轴相比，钢-CF/PEEK 复合轴在径向位移上显著降低，其中环向纤维取向的复合轴降低了 85.7%，交叉纤维取向的复合轴降低了 67.3%；轴向位移上，交叉纤维取向的复合轴降低了 11.5%。

关键词：热特性；钢-CF/PEEK 复合轴；激光辅助原位固化

Uncorrected